

## Strain sensing behaviors of epoxy nanocomposites with carbon nanotubes under cyclic deformation



Xiaohan Cao<sup>a</sup>, Xiangdong Wei<sup>a</sup>, Guojie Li<sup>a</sup>, Chao Hu<sup>a</sup>, Kun Dai<sup>a,b,\*</sup>, Jiang Guo<sup>c</sup>, Guoqiang Zheng<sup>a</sup>, Chuntai Liu<sup>a</sup>, Changyu Shen<sup>a</sup>, Zhanhu Guo<sup>c,\*\*</sup>

<sup>a</sup> School of Materials Science and Engineering, The Key Laboratory of Material Processing and Mold of Ministry of Education, Zhengzhou University, Zhengzhou, Henan 450001, PR China

<sup>b</sup> State Key Laboratory of Polymer Materials Engineering, Sichuan University, Chengdu, Sichuan 610065, PR China

<sup>c</sup> Integrated Composites Laboratory (ICL), Department of Chemical & Biomolecular Engineering, University of Tennessee, Knoxville, TN 37996, USA

### ARTICLE INFO

#### Article history:

Received 15 December 2016

Received in revised form

20 January 2017

Accepted 26 January 2017

Available online 30 January 2017

#### Keywords:

Epoxy nanocomposites

Piezoresistivity

Mechanical properties

### ABSTRACT

The strain sensing behavior of multi-walled carbon nanotubes (MWCNT)/epoxy (EP) conductive composites subjected to tensile strain was studied in detail. With increasing the load to rupture, the responsivity ( $\Delta R/R_0$ ,  $R_0$  is the original resistance,  $\Delta R$  is instantaneous change in resistance) increased in a linear fashion and then began to decrease at a critical strain ( $\epsilon_c$ ), which was remarkably different from the thermoplastic conductive composites only with a monotonic increase of the responsivity. It was attributed to the decrease of the nanotube contact points, the increase in the gaps before  $\epsilon_c$ , and the reorientation and violent alignment of nanotubes in the zones of high local deformation (after  $\epsilon_c$ ). In addition, when the extension-retraction cycles were applied, the values of max  $\Delta R/R_0$  showed a distinct tendency with different strains around the  $\epsilon_c$ . These behaviors were attributed to the competition of network destruction and reconstruction during the cyclic deformation. The mechanism of this unique sensing behavior was proposed as well.

© 2017 Elsevier Ltd. All rights reserved.

### 1. Introduction

Conductive polymer composites (CPCs) have attracted a great deal of scientific and industrial interests due to their popular applications and easy fabrication in many fields [1–3], such as electromagnetic interference (EMI) shielding [4–7], self-regulated heating materials [8,9] and sensors [10–13]. In terms of strain sensing, a wide range of applications have been demonstrated including: health monitoring [14,15], wearable electronics [16–19], movement sensors [20,21], etc. With increasing the commercial applications of these materials, easier fabrication method with a lower cost is required. Since the landmark paper by Iijima [22], carbon nanotubes (CNTs) have attracted a large amount of attention

due to their extraordinary mechanical, electrical, and thermal properties [23,24]. CPCs containing CNTs exhibit a variety of sensing performance when subjected to external strain, indicating that CNTs are ideal fillers for strain sensors [25–28]. In recent years, significant advances have been made in the CNTs/thermoplastic conductive composites as strain sensors. For example, Kuronuma et al. studied the strain sensing property of the polycarbonate/multi-walled carbon nanotubes (MWCNT) composites [29]. The developed analytical model could account for the strain-dependent electrical resistance behavior of the CNTs-based polymer composites. Pham et al. [30] studied the strain dependent resistivity of the poly (methyl methacrylate)/MWCNT composites. They found that a reversible resistivity response was observed at strains less than 1% and the strain sensitivity of the conductive composites can be tailored by controlling the MWCNT loading, degree of MWCNT dispersion, and composite fabrication process.

Aside from the investigations regarding strain sensing behaviors of the thermoplastic composites, less work on the thermosetting matrix based conductive composites has been reported. High-performance thermosetting strain sensors have aroused wide concerns due to their high strength and stiffness, excellent

\* Corresponding author. School of Materials Science and Engineering, The Key Laboratory of Material Processing and Mold of Ministry of Education, Zhengzhou University, Zhengzhou, Henan 450001, PR China.

\*\* Corresponding author. Integrated Composites Laboratory (ICL), Department of Chemical & Biomolecular Engineering, University of Tennessee, Knoxville, TN 37996, USA.

E-mail addresses: [kundai@zzu.edu.cn](mailto:kundai@zzu.edu.cn) (K. Dai), [zguo10@utk.edu](mailto:zguo10@utk.edu) (Z. Guo).

reversibility and reproducibility. Epoxy (EP) resin is one of the most important thermosetting resins with low cost, and has been widely utilized for industrial applications, such as coatings, adhesives, hardware components and semiconductor encapsulation owing to their desirable properties. The strain sensing behavior of EP based strain sensors have attracted great interests in recent academic research fields. For instance, Tung et al. [31] reported the piezoresistive mechanical sensing behaviors of graphene/EP nanocomposites. They presented the use of a dimethylbenzamide (DMBA)-based hardener to improve the dispersion of graphene nanosheets, the interface between fillers and matrices and the sensing properties. Wichmann et al. [32] studied the electromechanical responses of carbon black (CB) filled EP CPCs with low filler contents, and they found that the composites exhibited a pronounced dependency of the electrical resistivity with the mechanical load. With increasing the strain, the resistance change vs. stress curves passed through a critical point ( $\epsilon_c$ ), followed by a drastic decrease in the responsivity shortly before the final failure, which is explained by the tunneling model of Simmons [33].

The electrical response of the filler conductive network is known to be related to the structural evolution of the CPCs [34]. The comprehensive understanding of the relationship between electrical and mechanical properties of CPCs under cyclic load conditions was very meaningful for the design and practical applications of strain sensor materials. For example, Zhao et al. [35] studied the resistivity variation of the CB/polypropylene (PP) and CNTs/PP conductive composites subjected to tensile. They found that when 10 extension-retraction cycles were applied, for CB/PP, the ratio values of max and min responsivity increased gradually with increasing the cycle number; while for CNTs/PP, the values decreased. The difference mainly depended on the distinction in the dimension of conductive fillers, the interaction between fillers and matrix, and the hysteresis effect. The resistivity response under cyclic loading of the MWCNT/thermoplastic polyurethane (TPU) [36] and graphene/TPU [37] composite films have also been studied, the strain-dependent resistance showed good recoverability and reproducibility after stabilization by cyclic loading. Although electromechanical performance of the EP based CPCs have been investigated, few studies about resistance peak at a critical strain ( $\epsilon_c$ ) are reported [32], and the mechanism is not fully clear. The strain sensing behaviors at strains around  $\epsilon_c$  under cyclic extension-retraction conditions, which are important for the origin of novel sensing behavior, have not been studied either.

In this research, the EP conductive composites with uniform distribution of MWCNTs were prepared through a solution dispersion method [38]. The morphology and percolation behavior of MWCNT/EP composites was investigated firstly. An electrically responsive peak at a critical strain ( $\epsilon_c$ ) was observed during the electromechanical behavior study. The strain sensing behaviors of the composites were investigated in detail during 10 extension-retraction cycles with different applied strains around the critical strain  $\epsilon_c$ . The influence of the destruction-reconstruction competition of the conductive MWCNT networks on the strain sensing behavior was discussed. Furthermore, a model was proposed to explain the strain sensing mechanisms when the CPCs were applied under different strains.

## 2. Experimental

### 2.1. Materials

Amino MWCNT with an average diameter of 8–15 nm were supplied by Chengdu Organic Chemicals Co. Ltd., Chinese Academy of Sciences. EP resin (model LT-5078A) and hardener (model LT-5078B) were purchased from RuiGao New Materials Co. Ltd., China.

### 2.2. Preparation of MWCNT/EP composites

Different MWCNT concentrations were dispersed into EP using a solution dispersion method as described in our earlier research [38]. Briefly, the MWCNT (0, 0.0013, 0.0065, 0.013, 0.039, 0.065, 0.104, 0.13, 0.169 g for making the CNT loading of 0, 0.005, 0.025, 0.05, 0.15, 0.25, 0.4, 0.5, and 0.65 vol %) were first dispersed in acetone (40 mL) by sonicating for 30 min to form a homogeneous suspension. Then the suspension was mixed with quantitative EP (10 g) by stirring for 30 min and sonicating for another 30 min. The mixture was maintained in a vacuum oven to remove the acetone. Subsequently, the hardener (3 g) was added to the mixture at a stoichiometric ratio. After degassing, the mixture was poured into a mold and cured at a schedule: 25 °C for 24 h and then 80 °C for 8 h. The composites fabrication process was shown in Fig. 1. The mold used in this research was dumbbell-shaped.

### 2.3. Characterizations of materials

For the conductive properties test, the volume electrical conductivities higher than  $10^6 \Omega \text{ cm}$  were measured using a ZC-36 high-resistance meter (Shanghai Cany Precision Instruments Co. Ltd., China). The dimension of the sample for resistivity measurements was  $25 \times 5 \times 2 \text{ mm}^3$ . Mechanical tests were carried out on a displacement controlled Suns UTM2203 universal testing machine at different crosshead speeds (0.5, 3 and 10 mm/min) (Shenzhen Suns Co., Ltd. Stock Technology, China). The specimen setup for strain sensing test was displayed in Fig. 2a. During the mechanical test, the resistance of MWCNT/EP composites was recorded continuously with a computer coupled with a high resistivity meter (model TH2683, supplied by Changzhou Tonghui Electronics Co. Ltd., China). The schematic diagram of a sample for strain sensing test was displayed in Fig. 2b. Some samples were fractured after frozen in liquid nitrogen for 30 min, the fracture surfaces of the samples were sputtered with a layer of platinum and observed by using a field emission scanning electron microscope (FESEM, JSM-7500F, Japan). The MWCNT in acetone (0.3 wt% loading) was magnetically and ultrasonically stirred for 30 min at room temperature, respectively. Then epoxy resin was added into the mixture used the same preparation procedures as shown in Fig. 1. And finally it was placed in a vacuum oven at 80 °C for 24 h, without adding the curing agent, small amounts of the prepared samples were used to do the thermogravimetric analysis. (TGA, TA instruments, Q50, USA). The TGA was conducted on the cured pure epoxy and MWCNT/EP nanocomposites from 25 to 700 °C with a nitrogen flow rate of 60 mL/min and a heating rate of 10 °C/min.

## 3. Results and discussions

### 3.1. Morphology and electrical performance of CPCs

In order to understand the influence of MWCNT on the electrical properties and the strain sensing behavior of CPCs, it is necessary to investigate the morphology and percolation behaviors of MWCNT/EP composites firstly. Fig. 3 shows the FESEM micrograph of the fracture surfaces of the composite. It can be seen that the MWCNT are well-dispersed in the EP matrix.

The electrical performance of the composites was studied. The percolation curve of the composites is plotted in Fig. 4. It can be seen that the conductivity displays a dramatic increase of 7 orders of magnitude when the filler content exceeds 0.025 vol %. This sharp change in conductivity indicates the formation of percolating network (i.e. the percolation behavior) [39]. According to the classical percolation theory as stated in Equation (1):

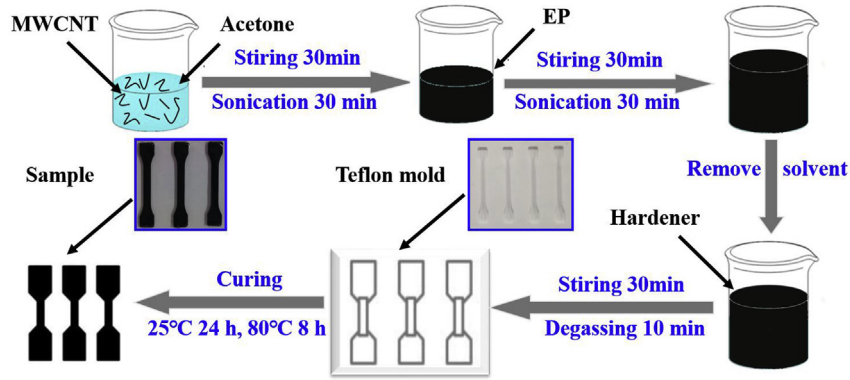


Fig. 1. Schematic illustration of the process for the preparation of MWCNT/EP composites.

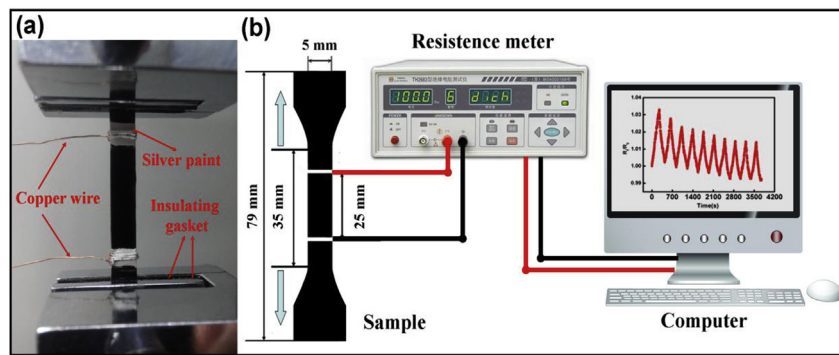


Fig. 2. (a) Sample setup for strain sensing test; (b) Schematic diagram of a sample for strain sensing test.

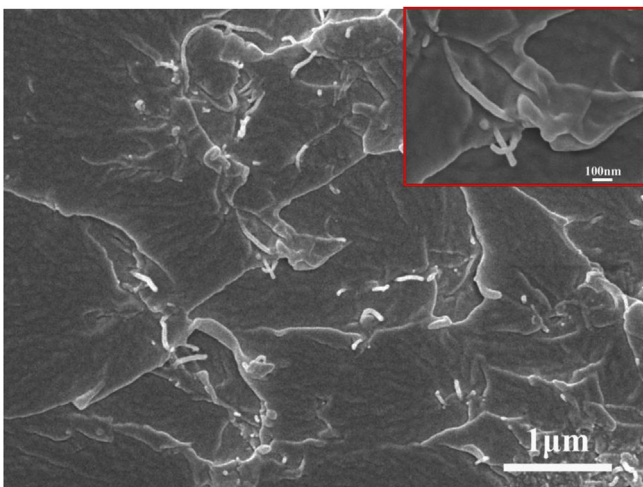


Fig. 3. FESEM micrograph of the morphology of the MWCNT/EP nanocomposites. The MWCNT concentration is 0.15 vol %.

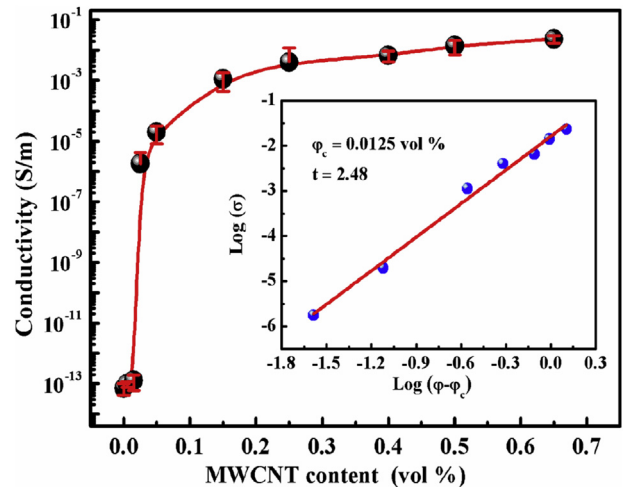


Fig. 4. Electrical conductivity vs. MWCNT contents of MWCNT/EP. Inset: log-log plot for  $\sigma$  vs.  $(\varphi - \varphi_c)$  for the same composites.

$$\sigma = \sigma_0(\varphi - \varphi_c)^t \quad (1)$$

where  $\sigma$  is the conductivity of the composite,  $\sigma_0$  and  $t$  are constants,  $\varphi$  is the filler content and  $\varphi_c$  is the percolation threshold. The percolation threshold of composites is ca. 0.0125 vol %, which is much lower than most of the reported values [40,41]. As shown in the inset of Fig. 4,  $t$  is estimated to be 2.48, implying the presence of a complex conductive network in the MWCNT/EP composites.

The lower percolation threshold of the MWCNT/EP is attributed

to the well-dispersed MWCNT and strong bonding between EP and MWCNT. FESEM micrographs (see Fig. 3) clearly show the good dispersion state of MWCNT in the EP matrix. The amidogen on the surface of the MWCNTs was used to tailor the interfacial interactions between MWCNT and EP matrix. The interfacial reaction took place between amine functional groups (both primary and secondary amines) of MWCNT and epoxide groups of EP, resulting in the ring-opening reactions followed by the cross-linking reactions (See Fig. 5) [42]. The TGA test was performed to investigate

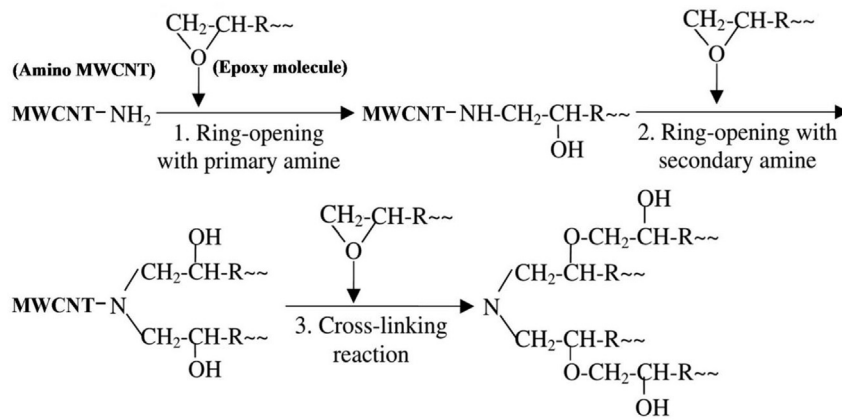


Fig. 5. Schematic of interfacial reactions between MWCNT and EP molecule.

the MWCNT/EP formation mechanism [43,44]. Fig. 6 shows the TGA curves of the MWCNT/EP and pristine EP. Both materials present similar decomposition profiles and two major degradation stages. The first stage is due to the degradation of the C–O–C group in the EP monomer and the second stage is from the degradation of the benzene ring. It is obvious that the thermal stability of the MWCNT/EP is better than that of the pristine epoxy, which might be related to the chemical bonding formed between amine functional groups of MWCNT and epoxide groups of EP [43–46]. The other possible reason for this increase is related to the improved thermo-oxidative stability of the EP especially in the vicinity of the nanotube surfaces, the origin is that the enhanced thermal conductivity owing to the incorporation of MWCNT can facilitate the heat transport [47].

It is reported that the responsivity to the tensile strain is more noticeable when the filler concentration is just beyond the percolation region [48]. Because at this concentration, any transformation of the inter-aggregate distance can generate a change in potential barrier that more easily makes the transport of charge carriers impossible, and as a result, a significant change in the resistivity will appear [49]. Therefore, for the strain sensing behaviors test in the present paper, the MWCNT concentration of 0.15 vol % is chosen for the tension test.

### 3.2. Stress-strain behaviors under different tensile speeds

Fig. 7a illustrates the typical stress-strain curves of the MWCNT/

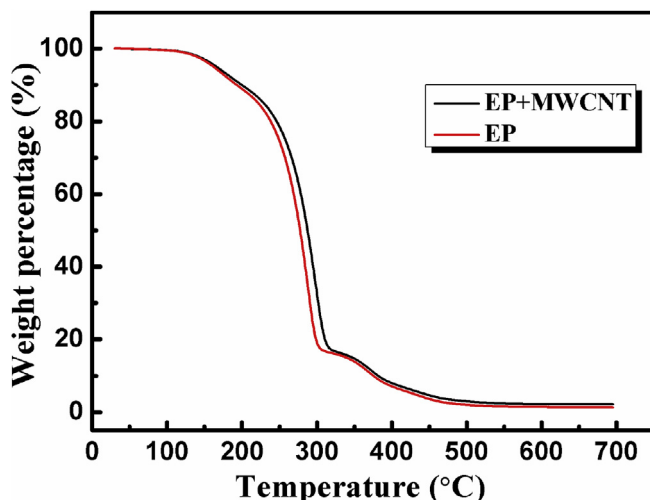


Fig. 6. TGA curves of pure EP and its MWCNT (0.15 vol %) composites.

EP composites with different tensile speeds. The instrumental software provides the additional values of mechanical properties such as tensile strength, elongation, and young's modulus (see Fig. 7b–d). Obviously, with increasing the tensile speed, the tensile strength of the composites increases, while the elongation decreases. The Young's modulus gradually increases with increasing the tensile speed. It is known that the motion of the macromolecular chain segments always cannot match the change rate of the stress, as a result, the macromolecular chain segments do not have enough time to relax when the tensile speed is too fast. In order to obtain a relatively larger deformation, a relatively lower tensile speed 0.5 mm/min is applied to study the electrical and mechanical responses of MWCNT/EP CPCs.

### 3.3. Electrical properties under tension

Fig. 8 displays the responsivity ( $\Delta R/R_0$ ,  $R_0$  is the original resistance,  $\Delta R$  is instantaneous change in resistance) and the corresponding stress as a function of strain for the MWCNT/EP composites. The results reveal a pronounced dependency of the electrical resistivity on the mechanical load. As can be seen, the stress increases linearly with increasing the strain. More interestingly, the responsivity increases in a linear fashion firstly and then decreases in exponential until the failure of the sample. As shown in Fig. 7, the blue line is the corresponding fitting of the responsivity. The linear increase of the responsivity before  $\epsilon_c$  is caused by the decrease of the nanotube contact points and the increase in the gaps, i.e. tunneling distance, resulting from the tension of sample. In this regime, the destruction of the sample and the conductive network in the EP matrix can be assumed to be synchronous. The in-situ relative resistance change resulting from elastic deformation can be described as [32]:

$$\frac{\Delta R}{R_0} \approx \exp[\gamma s_0 (\cos^2 \theta - \nu \sin^2 \theta) \epsilon] - 1 \quad (2)$$

$$\gamma = \frac{4\pi}{h} \sqrt{2m\zeta} \quad (3)$$

where  $s_0$  is the average interparticle distance in the unloaded state,  $\epsilon$  is the applied strain,  $m$  is the electron mass,  $h$  is the Planck's constant,  $\zeta$  is the height of the tunneling potential barrier and  $\theta$  is the average angle between the particle contact and the direction of applied load. It should be noted that at the beginning of the tension, the MWCNTs are very difficult to orientate due to their excellent molecular coupling with the polymer chains. As clearly suggested by Equation (2),  $\epsilon$  is the only contribution to diminish the

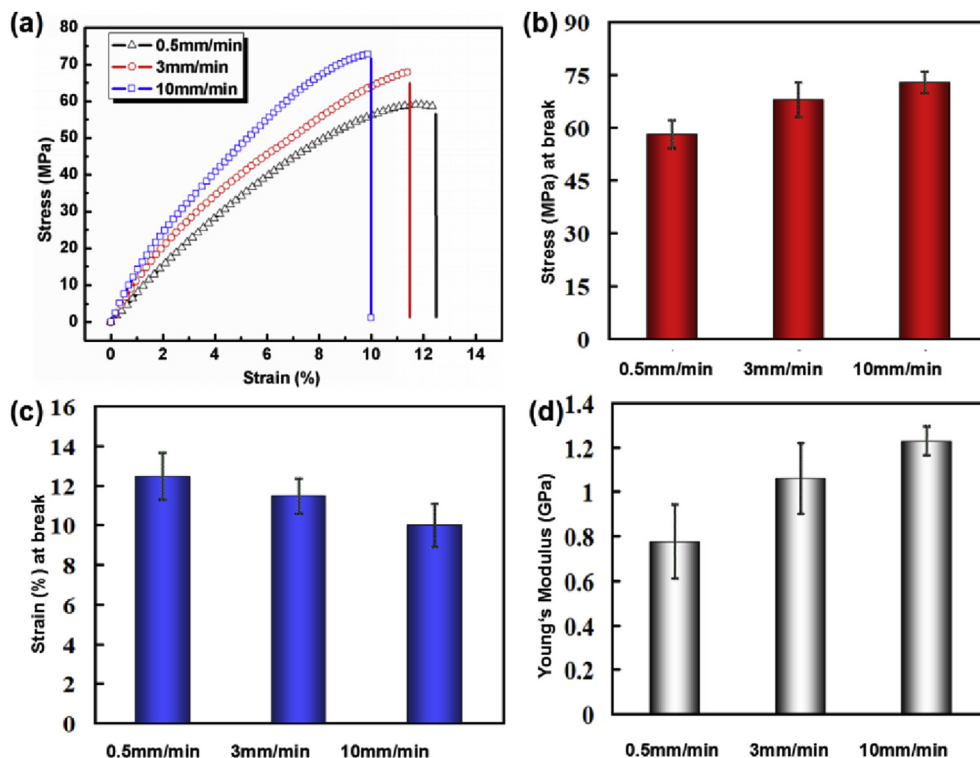


Fig. 7. (a) Stress-strain curves and representative bar diagrams of (b) tensile strength, (c) strain and (d) young's modulus of composites with 0.15 vol % MWCNT under different tensile speeds.

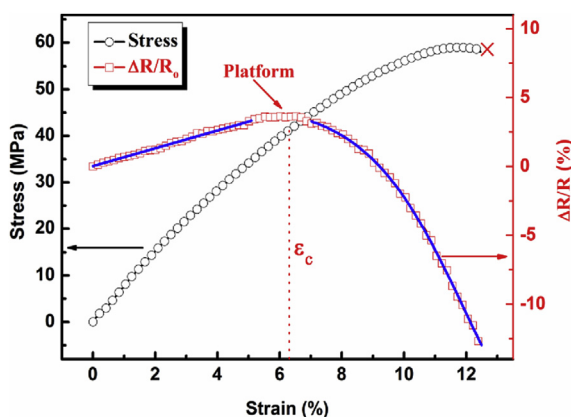


Fig. 8. In-situ relative resistance change and the corresponding stress as function of strain for the composites with 0.15 vol % MWCNT. The blue line is the fitting of in-situ relative resistance change. (For interpretation of the references to colour in this figure legend, the reader is referred to the web version of this article.)

conduction of the whole network. As a consequence, the responsivity increases with increasing the  $\epsilon$ .

Beyond the elastic regime, the viscoelastic and inelastic deformation processes occur in the composites, resulting in irreversible changes in the conductive network of conductive fillers. At the critical strain, a platform of  $\Delta R/R_0$  can be observed (see Fig. 8). This is due to the large aspect ratio and entanglement structure of MWCNT, resulting in a balance of the reconstruction and destruction of the conductive networks in the EP matrix under tension. It is known that the inelastic matrix deformation can result in an intensive rupture of the conducting networks. However, assisted by Poisson's contraction (the size reduction in transverse direction and the length increase along the tensile direction), the

reorientation and alignment of MWCNTs in the zones of high local deformation are generated [50]. Instead of a destruction of the conductive networks, the MWCNTs are able to come into a closer contact, giving rise to a platform of  $\Delta R/R_0$ . With increasing the applied strain, these rearrangement behaviors play a key factor in this system due to the nature of EP matrix and the structure of the network of MWCNT, such as aspect ratio, inter-particle interactions, etc., giving rise to the exponential decrease of the relative resistance. Important parameters should be the three-dimension crosslinking structure of EP resins and a good level of dispersion of MWCNT with high aspect ratio in the matrix, which benefit the reformation of the conductive networks. Furthermore, the evolution of the conductive network is influenced by the filler content obviously due to the change of the average interparticle  $s_0$  [32]. As shown in Fig. S1, it is found the value of the  $\epsilon_c$  ascends with increasing the MWCNT content. With increasing the MWCNT content, the average interparticle distance  $s_0$  (Eq. (2)) becomes smaller, the MWCNT conductive network thus becomes steadier and subsequently influences the strain sensing behaviors of the nanocomposite further. The MWCNT/EP needs to suffer a larger strain to approach the balance of the reconstruction and destruction of the steadier conductive network, resulting in a higher  $\epsilon_c$  of the composite with a higher MWCNT content of 0.25 vol % (Fig. S1).

We enumerate the in-situ relative resistance change of some CPCs based on different fillers or matrixes [32,34,35,51,52]. It is found that the EP based CPCs exhibit a different piezoresistive behavior when the filler is different [32,34]. It should be attributed to different structures of the network of conductive particles. However, for the thermoplastic based CPCs, the in-situ relative resistance change reveals a monotonic increase with increasing the strain without any discontinuity [35,51,52]. It can be explained by the tunneling mechanism, the increase of the distance between the conductive particles results in an obvious decrease of the

conductivity. From these results, it can be concluded that the piezoresistive behavior in CPCs mainly depends on both the microstructure of the conductive network and the nature of matrix.

In order to gain an insight into the reproducibility of the strain sensor and get further information about the microstructure development of MWCNT/EP CPCs in tension, 10 cycles with different applied strains and  $\Delta R/R_0$  vs. time of composites were investigated. The composites were strained and relaxed to their unloaded state cyclically for 10 times. The results are shown in Fig. 9. The increasing strain obviously enhances the irreversible deformation of the composites. Consequently, the residual strain increases in the unloaded state with increasing the number of cycles. As shown in Fig. 9a–c, the  $\Delta R/R_0$  increased with increasing the applied strain; and decreased with decreasing the strain. For CPCs during elongation, it is well recognized that two antagonistic phenomena occur simultaneously in the system: the destruction of existing conductive networks and the reconstruction of new conductive networks. When the sample is stretched, the MWCNTs move with the motion of the macromolecular network and pull apart, resulting in an increase of the inter-particle distance, increasing the relative resistance of the composites; when the sample is reverted, contrary to the stretch, the relative resistance of the composites decreases. Moreover, as the strain amplitude increases, the responsivity of the composites increases as well. From the result above, it should be also noticed that the max  $\Delta R/R_0$  cannot return to its original values after the first cycle (see Fig. 9b–d) due to the destruction or reconstruction of the conductive networks. It is attributed to the hysteresis effect of the composites and some irreversible deformation.

The normalized (i.e., divide the max  $\Delta R/R_0$  values by the max value of the first cycle) change in the max  $\Delta R/R_0$  of the MWCNT/EP

composites with different tensile strains during 10 cycles is shown in Fig. 10. For the strain amplitude of 2%, it can be seen that there is no obvious change of the max  $\Delta R/R_0$  values. That is because that this strain (2%) belongs to the linear elastic regime of the composites (see Fig. 8). In the elastic regime, the deformation of the sample occurs and thus the destruction of conductive networks in the matrix can be assumed to be reversible. The conductive networks can stay in the original morphology after a cyclic tension. As a consequence, the max  $\Delta R/R_0$  can return to their initial values. For the strain amplitude of 4%, Fig. 10, the max  $\Delta R/R_0$  values have a slight increase after the first cycle. This phenomenon might be ascribed to the irreversible destruction of the conductive networks.

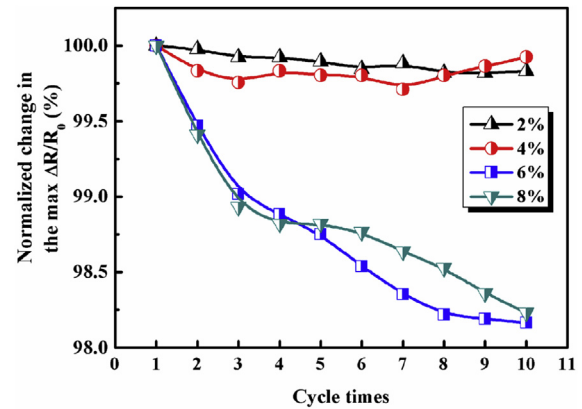


Fig. 10. Normalized change in the max  $\Delta R/R_0$  of MWCNT/EP composites with different tensile strain amplitudes during 10 cycles (MWCNT content 0.15 vol %).

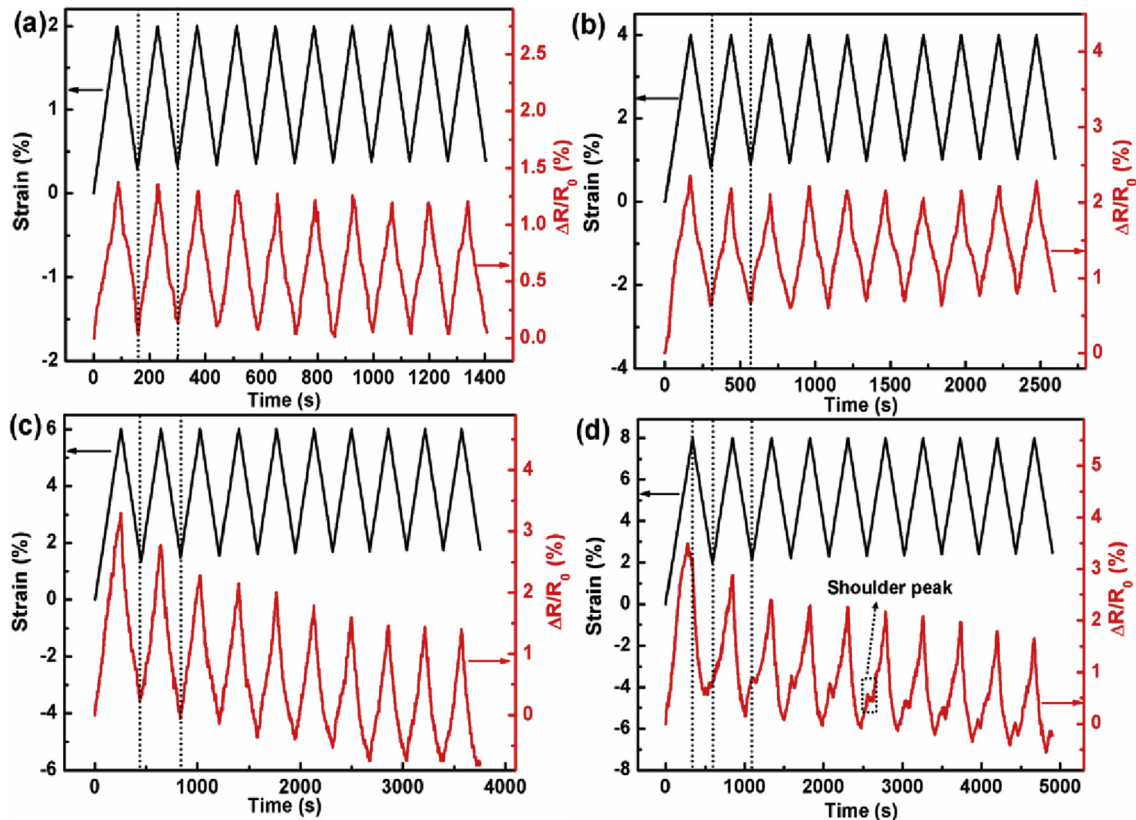


Fig. 9. Relationships of different tensile strains and  $\Delta R/R_0$  vs. time of composite with 0.15 vol % MWCNT during 10 extension-retraction cycles: with a strain amplitude of (a) 2%; (b) 4%; (c) 6%; (d) 8%.

This strain (4%) is beyond the scope of the elastic regime about 3%. As aforementioned, the destruction of conductive networks gradually plays a dominant role in this zone. In the extension process, the partially damaged conductive network will be a little broken further, leading to a slight increase of the max  $\Delta R/R_0$  during the following cycles.

For the strain amplitude of 6%, the max  $\Delta R/R_0$  values have a pronounced decrease with increasing the cycle number. The higher deformation of the composites leads to the rearrangement of MWCNTs and results in a better conductivity after each cycle along the tension direction. Given this dominance, it is not surprising to obtain a negative variation of the max  $\Delta R/R_0$  value. For the strain amplitude of 8%, the variation tendency of max  $\Delta R/R_0$  values is similar to strain 6%. However, the extent of the decrease is sharper than that obtained under the strain 6%. It is attributed to the excessive reconstruction of conductive paths because of the larger strain (8%). More interestingly, a slight deviation of the max  $R_t/R_0$  response to strain is observed in Fig. 9d, where  $\Delta R/R_0$  begins to decrease before the applied strain reaches the maximum (8%) (see the black dotted line). In other words, the relative resistance is not monotonic with respect to the applied strain because the maximum strain exceeds the  $\epsilon_c$ , and the relative resistance begins to decrease after  $\epsilon_c$  even the sample is still dragged. This result is in reasonable agreement with the analysis of Fig. 8. In addition, before the second loading, the min  $\Delta R/R_0$  value reaches the valley value and increases in a small range. This generates the formation of a new min and max  $\Delta R/R_0$  (called “shoulder peak”), and it appears after several cycles. This behavior is not obvious for lower strains, Fig. 9. This phenomenon was often explained by the competition between network destruction and reconstruction during the extension-retraction cycles of the composites [53]. A similar

phenomenon had been previously reported for the MWCNT/TPU composite films [36]. It was explained by the testing conditions (e.g. the testing strain) and the molecular structure (e.g. hard segments vs. soft segments, degree of cross-linking, etc.) of matrix. However, in the case of the MWCNT/TPU composites, the  $\epsilon_c$  does not appear even at a strain amplitude of 403% [52]. As a result, it can be speculated that this phenomenon is owing to the nature of EP matrix and the changing structure of the conductive network during the dynamic loading.

Based on the results and discussions, a schematic illustration was proposed to explain the mechanisms of the fantastic strain sensing behaviors of the MWCNT/EP composites shown in Fig. 11. The original conductive network (yellow line) before stretching is shown in Fig. 11a–c. It can be seen that MWCNTs (black line) with large aspect ratios are arranged in EP intricately. In Fig. 11a'–c', the number of conductive networks decreases due to the deformation of composites under tension with different strains. The applied higher strain can result in a more obvious decrease of the number of conductive networks, as a result, the  $\Delta R/R_0$  increases obviously with increasing the applied strain (see Fig. 9). For the unloaded state in a tensile process with 2% strain as shown in Fig. 11a'', there is no evident reconstruction or destruction of the conductive networks. The number of conductive networks has no change due to that fact that this strain (2%) belongs to the linear elastic regime. As a result, the max  $\Delta R/R_0$  values have no remarkable change. For the unloaded state in tensile process with 4% strain as shown in Fig. 11b'', the destruction of conductive networks are more predominant than the formation of new ones. As a result, the number of conductive paths decreases at the end of the cycle, giving rise to a slight increase of the max  $\Delta R/R_0$ . For the unloaded state in the tensile process with a higher strain (see Fig. 11c''), the number of

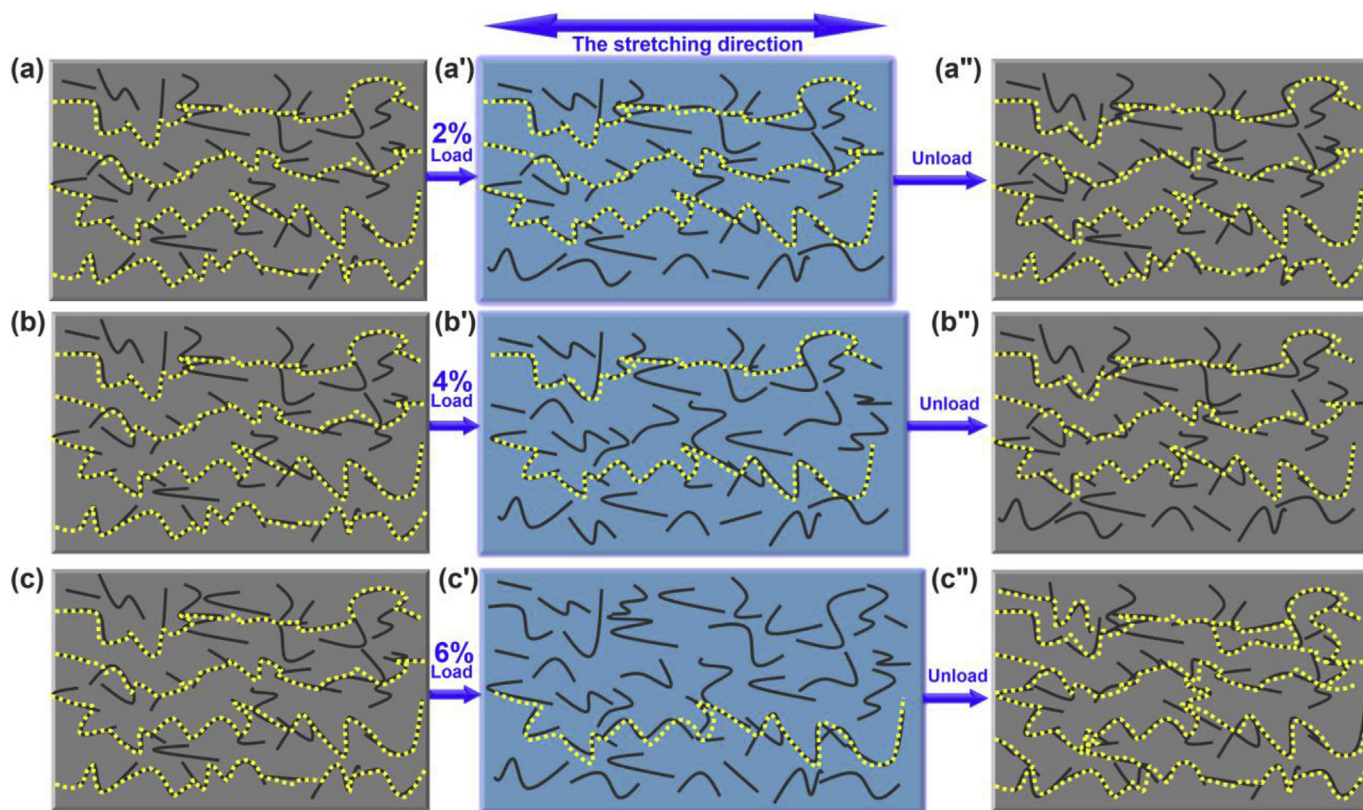


**Fig. 11.** Schematic illustration of influence of MWCNT structure on the strain sensing behavior of MWCNT/EP composites with different tensile strains: (a–c) initial state; (a'–c') the load state (with a strain amplitude of a' 2%; b' 4%; c' 6%); (a''–c'') final unload state. The black lines represent the MWCNT, the dotted yellow lines represent the formation or damage of the conductive paths. (For interpretation of the references to colour in this figure legend, the reader is referred to the web version of this article.)

conductive paths increases obviously along the tensile direction due to the orientation of the MWCNT in the EP matrix. Owing to the viscoelastic behavior of the polymer composites, some of these new formative conductive paths are preserved, and a much perfect conductive network is obtained along the tensile direction at the end of this cycle, leading to the distinct decrease of the max  $\Delta R/R_0$  values.

It is evident that different tensile strains around the  $\epsilon_c$  can result in different strain sensing behaviors of the MWCNT/EP composites. The mechanism of the difference as discussed above is meaningful for the long-term and cyclic applications of different strain sensors made from the MWCNT/EP CPCs. These results are useful in designing the EP based CPCs with different strain sensing capabilities to fulfill different requirements.

#### 4. Conclusion

Strain sensing behavior under different tensile strains of a MWCNT/EP composite with an ultralow percolation threshold (0.0125 vol %) was studied. It was found that the responsivity increases to its maximum value and then begins to decrease at a  $\epsilon_c$ . This phenomenon was attributed to the decrease of the nanotube contact points and the increase in the gaps before  $\epsilon_c$ , and the reorientation and alignment of nanotube took place dramatically in the zones of high local deformation (after  $\epsilon_c$ ). The strain sensing behaviors under 10 cyclic loading of the composites were also investigated. The values of the max  $\Delta R/R_0$  showed pronounced different trend. At a strain amplitude of 2%, the responsivity showed good recoverability and reproducibility because the conductive networks could stay the original morphology after the cyclic tension. Under the strain amplitude of 4%, the max  $\Delta R/R_0$  value had a slight increase after the first cycle. It was ascribed to the irreversible destruction of conductive networks resulting from the slippage of MWCNT and the residual strain of sample. When larger strains (6% and 8%) were applied, a negative variation of the max  $\Delta R/R_0$  value was obtained owing to the reconstruction of new conductive networks, and some of the new conductive paths were preserved at last due to the viscoelastic behavior of the composites. A model was proposed to illustrate the mechanism of the different sensing behaviors of the composites. Different sensing behaviors can be obtained around the  $\epsilon_c$  due to the distinct evolution of the conductive network. The fantastic strain sensing behaviors are meaningful for the design and application of EP based composite in crack detection, human-machine interactions and aircraft applications, etc.

#### Acknowledgements

The authors gratefully acknowledge the financial support of this work by National Natural Science Foundation Item (Contract Number: 51603193, 11572290, 11432003), National Natural Science Foundation of China-Henan Province Joint Funds (Contract number: U1604253), China Postdoctoral Science Foundation (Contract Number: 2015M580637, 2016T90675), Opening Project of State Key Laboratory of Polymer Materials Engineering (Sichuan University) (Contract Number: sklpm2016-4-21), Special Science Foundation for Excellent Youth Scholars of Zhengzhou University (Contract Number 1421320041). Z. Guo appreciates the start-up fund from University of Tennessee Knoxville.

#### Appendix A. Supplementary data

Supplementary data related to this article can be found at <http://dx.doi.org/10.1016/j.polymer.2017.01.068>.

#### References

- [1] J. Huang, Y. Zhu, W. Jiang, J. Yin, Q. Tang, X. Yang, Parallel carbon nanotube stripes in polymer thin film with remarkable conductive anisotropy, *ACS Appl. Mater. Inter.* 6 (3) (2014) 1754–1758.
- [2] C. Mao, J. Huang, Y. Zhu, W. Jiang, Q. Tang, X. Ma, Tailored parallel graphene stripes in plastic film with conductive anisotropy by shear-induced self-assembly, *J. Phys. Chem. Lett.* 4 (1) (2013) 43–47.
- [3] C. Mao, Y. Zhu, W. Jiang, Design of electrical conductive composites: tuning the morphology to improve the electrical properties of graphene filled immiscible polymer blends, *ACS Appl. Mater. Inter.* 4 (10) (2012) 5281–5286.
- [4] Y. Yang, M.C. Gupta, K.L. Dudley, R.W. Lawrence, Novel carbon nanotube-polystyrene foam composites for electromagnetic interference shielding, *Nano Lett.* 5 (11) (2005) 2131–2134.
- [5] Z. Zeng, H. Jin, M. Chen, W. Li, L. Zhou, Z. Zhang, Lightweight and anisotropic porous MWCNT/WPU composites for ultrahigh performance electromagnetic interference shielding, *Adv. Funct. Mater.* 26 (2) (2016) 303–310.
- [6] Y. Chen, H.-B. Zhang, Y. Yang, M. Wang, A. Cao, Z.-Z. Yu, High-performance epoxy nanocomposites reinforced with three-dimensional carbon nanotube sponge for electromagnetic interference shielding, *Adv. Funct. Mater.* 26 (3) (2016) 447–455.
- [7] S. Bose, M. Sharma, A. Bharati, P. Moldenaers, R. Cardinaels, A strategy to achieve enhanced electromagnetic interference shielding at ultra-low concentration of multiwall carbon nanotubes in PzMSAN/PMMA blends in the presence of a random copolymer PS-r-PMMA, *RSC Adv.* 6 (32) (2016) 26959–26966.
- [8] S. Isaji, Y. Bin, M. Matsuo, Electrical and self-heating properties of UHMWPE-EMMA-NiCF composite films, *J. Polym. Sci. Part B Polym. Phys.* 47 (13) (2009) 1253–1266.
- [9] J. Cui, D. Daniel, A. Grinthal, K. Lin, J. Aizenberg, Dynamic polymer systems with self-regulated secretion for the control of surface properties and material healing, *Nat. Mater.* 14 (8) (2015) 790–795.
- [10] T. Yamada, Y. Hayamizu, Y. Yamamoto, Y. Yomogida, A. Izadi-Najafabadi, D.N. Futaba, K. Hata, A stretchable carbon nanotube strain sensor for human-motion detection, *Nat. Nanotechnol.* 6 (5) (2011) 296–301.
- [11] H. Liu, J. Gao, W. Huang, K. Dai, G. Zheng, C. Liu, C. Shen, X. Yan, Z. Guo, Electrically conductive strain sensing polyurethane nanocomposites with synergistic carbon nanotubes and graphene bifillers, *Nanoscale* 8 (26) (2016) 12977–12989.
- [12] T.Q. Trung, S. Ramasundaram, B.U. Hwang, N.E. Lee, An all-elastomeric transparent and stretchable temperature sensor for body-attachable wearable electronics, *Adv. Mater.* 28 (3) (2016) 502–509.
- [13] F.R. Baptista, S.A. Belhout, S. Giordani, S.J. Quinn, Recent developments in carbon nanomaterial sensors, *Chem. Soc. Rev.* 44 (13) (2015) 4433–4453.
- [14] S. Gao, R. Zhuang, J. Zhang, J. Liu, E. Mader, Glass fibers with carbon nanotube networks as multifunctional sensors, *Adv. Funct. Mater.* 20 (12) (2010) 1885–1893.
- [15] S. Makireddi, S.S.G. Kosuri, F.V. Varghese, K. Balasubramanian, Electro-elastic and piezoresistive behavior of flexible MWCNT/PMMA nanocomposite films prepared by solvent casting method for structural health monitoring applications, *Compos. Sci. Technol.* 118 (2015) 101–107.
- [16] B.J. Munro, T.E. Campbell, G.G. Wallace, J.R. Steele, The intelligent knee sleeve: a wearable biofeedback device, *Sens. Actuat. B Chem.* 131 (2) (2008) 541–547.
- [17] X. Pu, L. Li, H. Song, C. Du, Z. Zhao, C. Jiang, G. Cao, W. Hu, Z.L. Wang, A self-charging power unit by integration of a textile triboelectric nanogenerator and a flexible lithium-ion battery for wearable electronics, *Adv. Mater.* 27 (15) (2015) 2472–2478.
- [18] J. Lee, H. Kwon, J. Seo, S. Shin, J.H. Koo, C. Pang, S. Son, J.H. Kim, Y.H. Jang, D.E. Kim, T. Lee, Conductive fiber-based ultrasensitive textile pressure sensor for wearable electronics, *Adv. Mater.* 27 (15) (2015) 2433–2439.
- [19] S. Hong, H. Lee, J. Lee, J. Kwon, S. Han, Y.D. Suh, H. Cho, J. Shin, J. Yeo, S.H. Ko, Highly stretchable and transparent metal nanowire heater for wearable electronics applications, *Adv. Mater.* 27 (32) (2015) 4744–4751.
- [20] L. Duan, S. Fu, H. Deng, Q. Zhang, K. Wang, F. Chen, Q. Fu, The resistivity-strain behavior of conductive polymer composites: stability and sensitivity, *J. Mater. Chem. A* 2 (40) (2014) 17085–17098.
- [21] D. Jung, J.M. Lee, S.Y. Gwon, W. Pan, H.C. Lee, K.R. Park, H.C. Kim, Compensation method of natural head movement for gaze tracking system using an ultrasonic sensor for distance, *Sensors* 16 (1) (2016) 110.
- [22] S. Iijima, Helical microtubules of graphitic carbon, *Nature* 354 (1991) 56–58.
- [23] J. Chen, X. Cui, Y. Zhu, W. Jiang, K. Sui, Design of superior conductive polymer composite with precisely controlling carbon nanotubes at the interface of a co-continuous polymer blend via a balance of  $\pi$ - $\pi$  interactions and dipole-dipole interactions, *Carbon* 114 (2017) 441–448.
- [24] J. Huang, C. Mao, Y. Zhu, W. Jiang, X. Yang, Control of carbon nanotubes at the interface of a co-continuous immiscible polymer blend to fabricate conductive composites with ultralow percolation thresholds, *Carbon* 73 (2014) 267–274.
- [25] C. Li, E.T. Thostenson, T.W. Chou, Sensors and actuators based on carbon nanotubes and their composites: a review, *Compos. Sci. Technol.* 68 (6) (2008) 1227–1249.
- [26] R.H. Baughman, A.A. Zakhidov, W.A. de Heer, Carbon nanotubes—the route toward applications, *Science* 297 (2002) 787–792.
- [27] B. Zhang, H. Wang, Y. Zhao, F. Li, X. Ou, B. Sun, X. Zhang, Large-scale assembly of highly sensitive Si-based flexible strain sensors for human motion

- monitoring, *Nanoscale* 8 (4) (2016) 2123–2128.
- [28] Z. Zhang, Q. Liao, X. Zhang, G. Zhang, P. Li, S. Lu, S. Liu, Y. Zhang, Highly efficient piezotronic strain sensors with symmetrical Schottky contacts on the monopolar surface of ZnO nanobelts, *Nanoscale* 7 (5) (2015) 1796–1801.
- [29] Y. Kuronuma, T. Takeda, Y. Shindo, F. Narita, Z. Wei, Electrical resistance-based strain sensing in carbon nanotube/polymer composites under tension: analytical modeling and experiments, *Compos. Sci. Technol.* 72 (14) (2012) 1678–1682.
- [30] G.T. Pham, Y.B. Park, Z. Liang, C. Zhang, B. Wang, Processing and modeling of conductive thermoplastic/carbon nanotube films for strain sensing, *Compos. Part B* 1 (39) (2008) 209–216.
- [31] T.T. Tung, R. Karunakaran, D.N.H. Tran, B.S. Gao, S. Nag-Chowdhury, I. Pillin, M. Castro, J.F. Feller, D. Losic, Engineering of graphene/epoxy nanocomposites with improved distribution of graphene nanosheets for advanced piezo-resistive mechanical sensing, *J. Mater. Chem. C* 4 (16) (2016) 3422–3430.
- [32] M.H. Wichmann, S.T. Buschhorn, J. Gehrmann, K. Schulte, Piezoresistive response of epoxy composites with carbon nanoparticles under tensile load, *Phys. Rev. B* 80 (24) (2009) 245437.
- [33] J.C. Simmons, Generalized formula for the electric Tunnel effect between similar electrodes separated by a thin insulating film, *J. Appl. Phys.* 34 (6) (1963) 1793.
- [34] W. Li, A. Dichiaro, J. Bai, Carbon nanotube-graphene nanoplatelet hybrids as high-performance multifunctional reinforcements in epoxy composites, *Compos. Sci. Technol.* 74 (2013) 221–227.
- [35] J. Zhao, K. Dai, C. Liu, G. Zheng, B. Wang, C. Liu, J. Chen, C. Shen, A comparison between strain sensing behaviors of carbon black/polypropylene and carbon nanotubes/polypropylene electrically conductive composites, *Compos. Part A* 48 (2013) 129–136.
- [36] R. Zhang, H. Deng, R. Valenca, J. Jin, Q. Fu, E. Bilotti, T. Peijs, Strain sensing behaviour of elastomeric composite films containing carbon nanotubes under cyclic loading, *Compos. Sci. Technol.* 74 (2013) 1–5.
- [37] H. Liu, Y. Li, K. Dai, G. Zheng, C. Liu, C. Shen, X. Yan, J. Guo, Z. Guo, Electrically conductive thermoplastic elastomer nanocomposites at ultralow graphene loading levels for strain sensor applications, *J. Mater. Chem. C* 4 (1) (2016) 157–166.
- [38] X. Cao, Y. Lan, Y. Wei, G. Zheng, K. Dai, C. Liu, C. Shen, Tunable resistivity-temperature characteristics of an electrically conductive multi-walled carbon nanotubes/epoxy composite, *Mater. Lett.* 159 (2015) 276–279.
- [39] B. Lundberg, B. Sundqvist, Resistivity of a composite conducting polymer as a function of temperature, pressure, and environment: applications as a pressure and gas concentration transducer, *J. Appl. Phys.* 60 (1986) 1074–1079.
- [40] N. Li, Y. Huang, F. Du, X. He, X. Lin, H. Gao, Y. Ma, F. Li, Y. Chen, P. Eklund, Electromagnetic interference (EMI) shielding of single-walled carbon nanotube epoxy composites, *Nano Lett.* 6 (6) (2006) 1141–1145.
- [41] L. Guadagno, B. De Vivo, A. Di Bartolomeo, P. Lamberti, A. Sorrentino, V. Tucci, L. Vertuccio, V. Vittoria, Effect of functionalization on the thermo-mechanical and electrical behavior of multi-wall carbon nanotube/epoxy composites, *Carbon* 49 (6) (2011) 1919–1930.
- [42] P.C. Ma, S.Y. Mo, B.Z. Tang, J.K. Kim, Dispersion, interfacial interaction and re-agglomeration of functionalized carbon nanotubes in epoxy composites, *Carbon* 48 (6) (2010) 1824–1834.
- [43] H. Gu, S. Tadakamalla, Y. Huang, H.A. Colorado, Z. Luo, N. Haldolaarachchige, D.P. Young, S. Wei, Z. Guo, Polyaniline stabilized magnetite nanoparticle reinforced epoxy nanocomposites, *ACS Appl. Mater. Inter.* 4 (10) (2012) 5613–5624.
- [44] H. Gu, S. Tadakamalla, X. Zhang, Y. Huang, Y. Jiang, H.A. Colorado, Z. Luo, S. Wei, Z. Guo, Epoxy resin nanosuspensions and reinforced nanocomposites from polyaniline stabilized multi-walled carbon nanotubes, *J. Mater. Chem. C* 1 (4) (2013) 729–743.
- [45] J. Zhu, S. Wei, J. Ryu, M. Budhathoki, G. Liang, Z. Guo, In situ stabilized carbon nanofiber (CNF) reinforced epoxy nanocomposites, *J. Mater. Chem.* 20 (23) (2010) 4937.
- [46] X. Zhang, Q. He, H. Gu, H.A. Colorado, S. Wei, Z. Guo, Flame-retardant electrical conductive nanopolymers based on bisphenol F epoxy resin reinforced with nano polyanilines, *ACS Appl. Mater. Inter.* 5 (3) (2013) 898–910.
- [47] S.T. Huxtable, D.G. Cahill, S. Shenogin, L. Xue, R. Ozisik, P. Barone, M. Usrey, M.S. Strano, G. Siddons, M. Shim, P. Keblinski, Interfacial heat flow in carbon nanotube suspensions, *Nat. Mater.* 2 (11) (2003) 731–734.
- [48] A. Fathi, K. Hatami, B.P. Grady, Effect of carbon black structure on low-strain conductivity of polypropylene and low-density polyethylene composites, *Polym. Eng. Sci.* 52 (3) (2012) 549–556.
- [49] T. Del Castillo-Castro, M. Castillo-Ortega, P. Herrera-Franco, Electrical, mechanical and piezo-resistive behavior of a polyaniline/poly(n-butyl methacrylate) composite, *Compos. Part A* 40 (10) (2009) 1573–1579.
- [50] J.J. Ku-Herrera, F. Avilés, Cyclic tension and compression piezoresistivity of carbon nanotube/vinyl ester composites in the elastic and plastic regimes, *Carbon* 50 (7) (2012) 2592–2598.
- [51] L. Liu, D. Zhang, The sensitive electrical response of reduced graphene oxide-polymer nanocomposites to large deformation, *Compos. Part A* 75 (2015) 46–53.
- [52] P. Slobodian, P. Riha, P. Saha, A highly-deformable composite composed of an entangled network of electrically-conductive carbon-nanotubes embedded in elastic polyurethane, *Carbon* 50 (10) (2012) 3446–3453.
- [53] K. Yamaguchi, J. Busfield, A. Thomas, Electrical and mechanical behavior of filled elastomers. I. The effect of strain, *J. Polym. Sci. Part B Polym. Phys.* 41 (2003) 2079–2089.